



## Research Article

# Morphological transition of silicate crystals solidified from highly undercooled aerodynamically levitated melt droplets



Ganesh Shete<sup>1</sup> · Shyamprasad Karagadde<sup>1</sup> · Atul Srivastava<sup>1</sup>

Received: 15 July 2020 / Accepted: 15 January 2021 / Published online: 27 January 2021

© The Author(s) 2021 [OPEN](#)

## Abstract

The present work reports the morphological transition during solidification of a non-metallic system. Pure magnesium silicate ( $Mg_2SiO_4$ ) is chosen as the model material and the solidification experiments have been conducted under purely non-contact conditions using the principles of aerodynamic levitation. The influence of the undercooling and cooling rates on the surface features observed in the solidified samples is investigated. Levitation experiments have been performed for different samples, which are solidified for a range of undercooling levels between 360 to 1100° C. In order to understand and report the morphological transitions, solidified samples have been observed using scanning electron microscopy, which showed the formation of highly branched faceted microstructure for an undercooling regime of 360–800° C, and non-dendritic microstructure for even higher undercooling regime of 800–1100° C. Further experiments performed on this non-metallic system for different cooling rates also suggested that, regardless of the cooling rate, lower undercooling leads to branched faceted features, whereas higher undercooling results into unbranched facets. The methodology and instrumentation provide unique capabilities to probe the behavior of materials at high temperatures.

**Keywords** Solidification · Container-less conditions · Aerodynamic levitation · Non-metallic systems · Morphological transition

## 1 Introduction

The phenomenon of solidification from high-temperature melts holds importance in a range of scientific and technological applications. The spectrum of applications encompasses industrial sectors (such as turbine blades, high power lasers, electronic equipment), engineering (material science, etc.) and applied sciences (geophysics, earth and planetary sciences etc.). The morphology of the microstructure of metals, alloys, semiconductor materials depends heavily on thermal parameters such as bulk undercooling and cooling rate. Considering the inherent advantages associated with experiments under container-less conditions, various techniques such as electromagnetic levitation (EML), electrostatic levitation (ESL) and

aero-acoustic levitation have been adopted to study the high-temperature solidification phenomena at relatively higher levels of undercooling. However, such levitation techniques are limited by the nature of the material. The application of EML to study the morphological transition of metallic [1, 2] and semiconductor systems [3, 4] at different levels of undercooling can be seen in the open literature. Despite the presence of aforementioned literature on several metallic systems, the efforts made towards understanding the morphological transition of non-metallic systems under container-less conditions are rather limited. One of the primary motivations of performing such non-contact experiments on non-metallic systems (primarily on magnesium silicates) has been their relevance in the area of earth and planetary science. Magnesium silicate

✉ Atul Srivastava, [atulsr@iitb.ac.in](mailto:atulsr@iitb.ac.in); [atuldotcom@gmail.com](mailto:atuldotcom@gmail.com) | <sup>1</sup>Department of Mechanical Engineering, Indian Institute of Technology Bombay, Powai, Mumbai 400076, India.



(in crystalline as well as in amorphous state) has been found to be one of the major compositional constituents of meteorites (chondrules) [5, 6]. Chondrules are the main components of natural meteorites, and hence are considered to carry important information about the plausible formation conditions of the early solar system [7]. Being spherical in shape (diameter  $\approx 1$  mm), the chondrules are believed to be formed as a result of the high temperature crystallization process of magnesium silicate material under freely floating conditions [8]. Both contact as well as contact-less experimental configurations have been attempted in the past.

The conventionally-employed sample holding techniques limit the amount of undercooling that can be achieved during experiments due to the presence of an immediate nucleation site offered by the sample holder. For instance, the sample holding technique-based experimental study investigating the surface features of Olivine as the non-metallic system was limited to an undercooling level of 400 °C. Karina et al. [12] presented the melting of olivine samples by means of CO<sub>2</sub> laser and obtained textures such as barred olivine, olivine and pyroxene porphyritic chondrules of ordinary chondrites. Faure et al. [13] performed high-temperature crystallization experiments with sample holder technique, which offered heterogeneous condition at various undercoolings and cooling rates. Gucsik et al. [14] investigated cathodoluminescence microcharacterization of forsterite, which was grown with undercooling levels between 50–400 °C and found texture such as star-type feature, dendritic feature. Nicollet et al. [15] performed dynamic crystallization experiments and showed that the polyhedral olivine shape progressively changes to a skeletal and then to a dendritic morphology. Faure et al. [16] performed experiments to obtain thin dendrites at relatively lower undercooling of ( $156 < \Delta T < 356$  °C) and cooling rates as low as 1890 °C/h. These studies available in the literature show that the importance of developing an understanding of the morphological transitions of non-metallic systems (for instance, forsterite) has been realized by various researchers. However, the levels of undercooling achieved/realized in these reported experimental studies have primarily been restricted to relatively low values i.e. till  $\sim 400$  °C and not beyond. This limitation arises due to the direct contact of the molten material with an external surface that acts as the site of heterogeneous nucleation. Possibly, to overcome such limitations, the idea of performing such experiments under completely non-contact conditions has attracted the attention of the researchers in recent years.

In the context of experiments under non-contact conditions with non-metallic systems, for instance, magnesium silicate, a select group of researchers have made use of the concept of gas jet levitation. In this direction,

Srivastava et al. [9] performed crystallization experiments on forsterite under container-less conditions for different undercooling levels ranging up to 400 °C. Pack et al. [10] aerodynamically levitated and heated oxides and silicates at high temperatures to prepare the samples for microchemical analyses and also for evaporation and reduction experiments. Beitz et al. [11] developed an experimental setup having levitation nozzle to test the hypothesis that accretionary rims around chondrules were formed in the solar nebula by the accretion of dust on the surfaces of hot chondrules while levitated with the inert gas flow at room temperature 20 °C and at 1100 °C.

It is pertinent to note here that while the levitation based experimental studies are highly scarce, some attempts have indeed been made through numerical simulations by a select group of researchers. Recently, numerical simulations carried out for forsterite at various values of undercooling between 200–600 °C have revealed various morphological features such as dendritic structure, rim like structure, dendrites with rim structure and parallel dendrites structure [17, 18]. However, with these simulations, the capture of both dendritic and faceted morphologies is very challenging, and also need real-time experimental validation. A critical examination of these observational and theoretical studies performed on non-metallic systems shows that, the primary interest of the researchers has been to produce the morphological textures of solidified samples that bear similarities with the textures found in natural samples of chondrules. However, detailed analysis of the surface features with a focus on the morphological transitions, as a function of operating parameters such as level of relatively higher undercooling and relatively higher cooling rates (as compared to available literature), especially under non-contact conditions, has not been adequately addressed in the available literature.

The present work is an attempt towards bridging such research gaps and develop an understanding of the phenomenon of crystallization of high-temperature melt droplet with a focus on morphological transitions for a range of bulk undercooling (as high as 1100 °C) and cooling rates under non-contact conditions. The cooling rates that the samples have been subjected to in the present study are significantly higher than those employed in the previous experimental works reported by other researchers in this field. The non-contact conditions have been achieved by aerodynamically levitating the molten drops of magnesium silicate. The levitation technique suppresses the chances of heterogeneous nucleation and allows the realization of relatively higher levels of undercooling than the levels that can be achieved with the sample holding technique. High-temperature solidification experiments have been performed for various undercooling levels and cooling rates. Surface feature characterization of the solidified samples, obtained as a function of

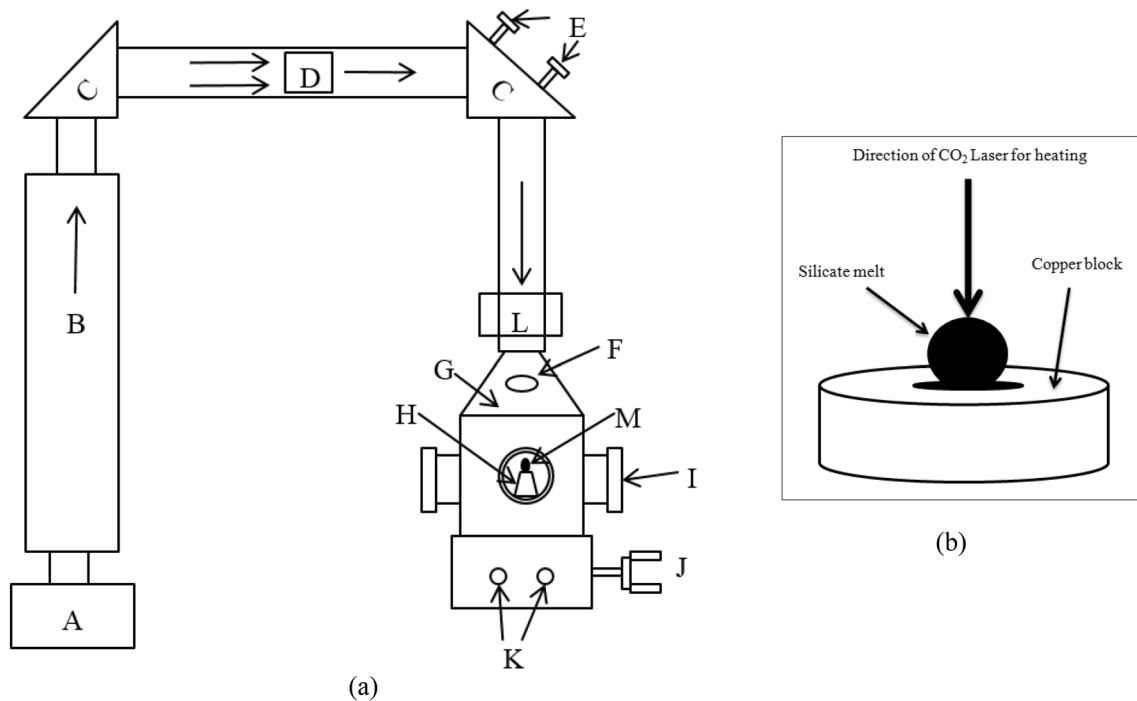


**Fig. 1** **a** Schematic of the complete levitation setup showing the important devices. A-Laser power supply (Synrad i401), B-Laser head, C-Mirror, D-Lens assembly, E-Laser beam focusing screws, F-Pyrometer ports, G-Process chamber, H-Nozzle, I-Optical ports,

J-Gas ports, K-Cooling water ports. L-Zn-Se window, M- Forsterite (Mg<sub>2</sub>SiO<sub>4</sub>) sample. **b** Schematic diagram showing the method of preparation of silicate spherules, consisting of a copper block hearth

these process parameters, has been carried out using scanning electron microscopy (SEM). A regime map depicting the morphological transitions of the solidified samples as a function of level of undercooling is presented for the first time in the current work.

The present manuscript is divided into 4 sections: Sect. 1 introduced the physical phenomena under study along with a discussion on some of the important works reported in the open literature. Based on the literature covered, motivation and objectives of the present research have been highlighted in this section. Details of experimental methodology, materials and methods etc. have been presented in Sect. 2. Primary findings of the work have been reported in Sect. 3 wherein the plausible role(s) of process parameters such as deep undercooling levels and cooling rates during morphological transitions of solidifying samples have been discussed. The manuscript is concluded in Sect. 4 wherein major conclusions of the present study have been drawn and its future prospects have been briefly discussed.

## 2 Experimental setup

### 2.1 Levitator setup

Non-contact solidification experiments on magnesium silicate spherules of  $\approx 2\text{--}3$  mm in diameter were performed using the principle of aerodynamic levitation of these samples. The levitation system makes use of an inert gas (Argon) to levitate the sample during the course of experimental run time. A schematic diagram of the complete experimental facility is shown in Fig. 1a. Synrad i401 high power continuous wave CO<sub>2</sub> laser (A) (maximum power = 400 W and wavelength = 10.6  $\mu\text{m}$ ) is employed as the heating source to raise the temperature of the sample and convert it into its molten state while keeping the sample under levitating condition. The laser beam is steered by a molybdenum mirror (C) and focused by lens assembly to strike on the target

(magnesium silicate sample) that is levitated inside the levitator chamber. The mirrors have alignment screws (E) for fine-tuning the path of the laser beam inside the chamber and the lens (D) helps to focus the beam at the desired point. This assembly is crucial in controlling the temperature of the molten droplet during experiments. The process chamber (G) (shown in Fig. 1a) comprises of a vessel which has a cylindrical bottom and a conical top part. The cone is connected to a cylindrical tube on the top that connects to the laser beamline.

The whole system starting from the laser beam stirring arrangement to the cylindrical tube connected to the process chamber together constitutes an enclosed beam delivery system. The levitation is carried out by letting the Argon gas flow through a conical nozzle (H). This nozzle is fixed on a base (as shown in Fig. 1a), which has a gas inlet (J) that allows two gases, if required, to flow through the nozzle at a specific ratio (set by a controller). Also, the base has got a liquid cooling system (K) that maintains the inlet gas at a set temperature. This same cooling system also cools the levitation chamber. The complete unit of the levitation gas flow, cooling temperature and the output of the laser is controlled by a computer integrated with the setup. The solidification phenomenon has been captured, in real-time, using a CMOS-based color camera (Model: BFLY-U3-23S6C). Videographic images were recorded at a frame rate of 30 fps and a spatial pixel resolution of  $572 \times 584$  (with 1 pixel being equal to  $5.86 \mu\text{m}$ ). Under standard conditions, the camera can operate at 41 fps at a maximum pixel resolution of  $1920 \times 1200$ .

## 2.2 Materials and methods

Pure forsterite ( $\text{Mg}_2\text{SiO}_4$ ) has been used as the non-metallic model system as the starting material in the present experiments.<sup>1</sup> Silicate solid spherules of diameters  $\sim 2\text{--}3 \text{ mm}$  are prepared in a laser hearth equipped with the experimental facility, and used as sample material, as shown in Fig. 1b. In this, the  $\text{CO}_2$  laser strikes the silicate powder and heats this powder above its melting point. The moment when powder transforms into a completely molten state, it is allowed to cool down by switching off the laser power and subsequently, due to surface tension forces, the sample acquires spherical shape in the circular groove (approximately of 4 mm diameter) created on the copper block (Fig. 1b). Samples are heated by focused radiation

of continuous-wave  $\text{CO}_2$  laser (*Firestar i400*,  $\lambda = 10.6 \mu\text{m}$  and spot size = 1 mm, maximum power output of 400 W), which has been integrated with the system. Considering the various heat transfer processes associated with the phenomena, a physical estimate of the total thermal energy required to convert the initially solid spherule into its complete molten state can be made. For the experiments reported, the total thermal power required for melting the forsterite samples was found to be close to 80 W. Factoring some of the other unavoidable losses of laser power (for instance, any loss in the optics-based beam guiding unit etc.), the net laser power deposited on the sample was kept slightly higher than the above mentioned physical estimate. Mass flow controllers are used to deliver gases to the levitation nozzle, and use of these mass flow controllers enables the production of a gas mixture over a range of 1–100% of gases at different flow rates. Sample temperature is measured by Chino IR-CAS optical pyrometer that operates near infrared wavelength (about  $0.9 \mu\text{m}$ ). The default acquisition rate of pyrometer is 10 Hz. This pyrometer is mounted on a gimbal and can be manually aligned and focused before the start of the experiment. The levitator has a built-in computer-controlled gas flow system. This system uses two 2000 SCCM flow meters and one 50 SCCM flow meter. These flow meters are configured to allow metering of single and two gas mixtures in ratio up to 100:1 of any two gases. A  $90^\circ$  opening angle nozzle has been employed to stably levitate the sample during its molten state.

After finishing the solidification experiments, SEM analysis of resultant crystallization structures of forsterite samples has been carried out using the JEOL 7600 SEM. In view of the fact that forsterite is electrically non-conductive, as part of sample preparation for SEM analysis, a thin gold–palladium coating has been applied on the sample in a vacuum chamber to reduce charging by creating a conductive surface. Images were acquired at 15 kV, 30 nA, with a  $90 \mu\text{m}$  aperture for microscopic observation of surface features. The images were taken at different magnifications to observe various features.

## 3 Results and discussion

Figure 2a shows the temperature–time history of the solidifying sample as it is allowed to cool down from its initial molten state, while being maintained under container-less conditions. The snapshots of the image sequence recorded during the transient process have also been shown at various important stages of the solidification process. At any given instant, the molten droplet can be clearly seen levitating under purely non-contact conditions (see Fig. 2b). It is to be mentioned that the solid spherule was converted

<sup>1</sup> Crystallinity of the sample was ascertained by carrying out XRD analysis of the initial samples and was confirmed to be of forsterite composition. All of the reflections of the XRD pattern could be indexed to display the existence of a pure orthorhombic phase of forsterite ( $\text{Mg}_2\text{SiO}_4$ ). Other phases such as enstatite were below the limit of detection or absent.

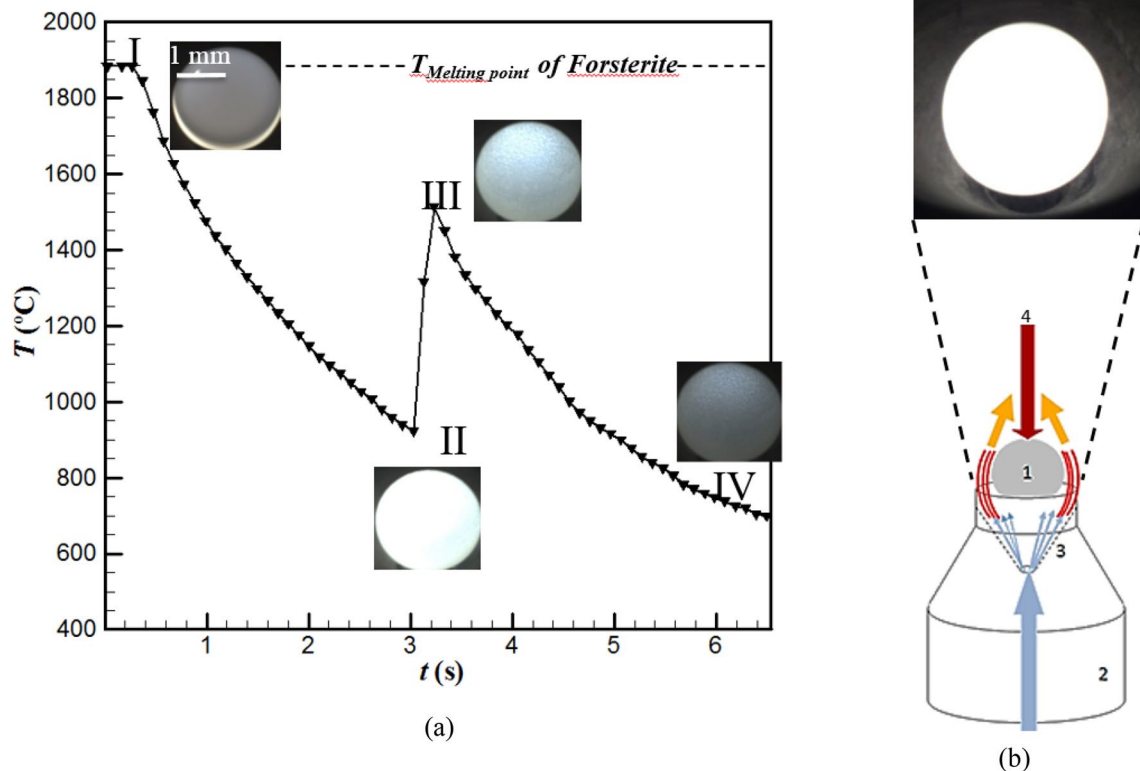


**Fig. 2** **a** Cooling curve of the droplet images for different temperatures. (From point I to II) In order to initiate the crystallization phenomenon, the laser power is reduced (either turned off to achieve quenching of the molten droplet and/or provided a well-defined cooling rate). (From point II to III) Recalcescence can clearly be seen wherein a sharp peak in the temperature profile is evident at the time instant that corresponds to the start of the crystallization process. (From point III to IV) Thereafter, it is allowed to cool down. **b**

Representative schematic of levitator system where 1, 2, 3 and 4 respectively indicate the levitating forsterite sample, nozzle body, Argon gas flow and CO<sub>2</sub> laser beam direction. The zoomed-in view in **b** shows one of the instantaneous videographic images of the levitated molten droplet. It can be seen that the molten spherule is under non-contact conditions and does not touch the surrounding nozzle surface

into a molten droplet by raising its temperature much above its melting point temperature ( $\approx 1890^\circ\text{C}$ ) using the focused radiation of continuous-wave 400 W CO<sub>2</sub> laser ( $\lambda = 10.6\ \mu\text{m}$  and spot size = 1 mm). As shown in Fig. 2a, the heating conditions were maintained for a considerably longer period of time so as to ensure a uniform and complete melting of the entire solid spherule (In Fig. 2a,  $t = 0$  corresponds to an arbitrary time instant just after which the cooling of the molten droplet was initiated). In order to initiate the solidification phenomenon, the laser power is reduced (either turned off to achieve quenching of the molten droplet and/or provide a well-defined cooling rate). As can be seen from the figure, the initial temperature of the spherule is close to  $2000^\circ\text{C}$ , thereafter, it is allowed to cool down. In view of the fact that the molten droplet has been maintained under non-contact conditions, an undercooling ( $\Delta T$ ) range as high as  $\approx 1100^\circ\text{C}$  could be achieved before the molten material started to crystallize. It was observed that the crystallization of the molten material starts at temperatures close to  $\approx 800^\circ\text{C}$

(see Fig. 2a Point II). The onset of crystallization is accompanied by a sudden change in the temperature of the molten material due to the release of the latent heat of crystallization. The signature of the release of latent heat of crystallization (also known as recalcescence) can clearly be seen from the cooling curve shown in Fig. 2a, wherein a sharp peak (from point II to III) in the temperature profile is evident at the time instant that corresponds to the start of the crystallization process. Once the heat released during the period of recalcescence gets dissipated and/or distributed throughout the volume of the molten droplet, the temperature follows a well-defined cooling rate till the crystallization process gets completed (point IV).

It is worth clarifying here that in contrast to the conventional approach wherein the nucleation is heterogeneously initiated (for instance, by deliberately allowing the sample to come in contact with an external surface at any given temperature below the liquidus temperature of the sample), the undercooling levels achieved in the present set of experiments, conducted in purely

container-less conditions, are primarily governed by the stochastic nature of the nucleation phenomena. For these reasons, multiple number of experiments, covering a large range of undercooling levels spanning from  $\sim 360^\circ\text{C}$  (near theoretical hypercooling limit of forsterite) to  $1100^\circ\text{C}$ , were performed on a large set of specimens, all of which were prepared from the same starting powder and following the same preparation methodology. For the majority of experiments, the undercooling levels achieved in the present work are well above the hypercooling limit ( $\Delta T_{hyp} = \Delta H_f / C_p$  where,  $\Delta H_f$  is the enthalpy of crystallization and  $C_p$  is the specific heat of liquid). The value of hypercooling limit  $\Delta T_{hyp}$  for forsterite melt is close to  $425^\circ\text{C}$  [6, 17]. The solidification process is known to change abruptly beyond this limit [17, 18]. When  $\Delta T < \Delta T_{hyp}$ , small amount of liquid fraction will be available even after recalescence since the temperature approaches the melting point at the end of solidification (due to the release of latent heat of crystallization). This liquid is solidified after the recalescence is over and such a process is generally referred to as the filling-in process [17]. However, when  $\Delta T > \Delta T_{hyp}$  (as considered for the present study), the temperature of the melt droplet neither exceeds nor approaches the melting point temperature at the end of recalescence. To the best of our knowledge, experimental works concerned with understanding the solidification phenomena and the associated morphological transitions of such deeply undercooled (with undercooling levels higher than the hypercooled limit) forsterite molten droplets are highly scarce in the open literature, which, in turn, emphasizes the importance and novelty of the present work.

It is pertinent to mention here that the undercooling levels reported in the present work correspond to those experimental runs that showed maximum repeatability. Furthermore, repeated experiments on the same droplet showed more or less the same undercooling on a consistent basis until its size remained large enough to be successfully levitated, as the sample exhibited some evaporative mass loss in every experiment. In order to ascertain that the evaporative losses of composition at such elevated temperatures were not very significant, necessary tests such as XRD analysis, checking the size of the solidified samples etc. were performed after every experimentation. In particular, the XRD analysis ruled out the presence of any extra phase in the solidified samples. Other tests also confirmed that mass (composition) changes of the samples due to evaporative losses were negligible.

### 3.1 Observations of surface features at varying levels of undercooling

In the present work, the aerodynamic levitation of forsterite samples enabled the measured undercooling levels

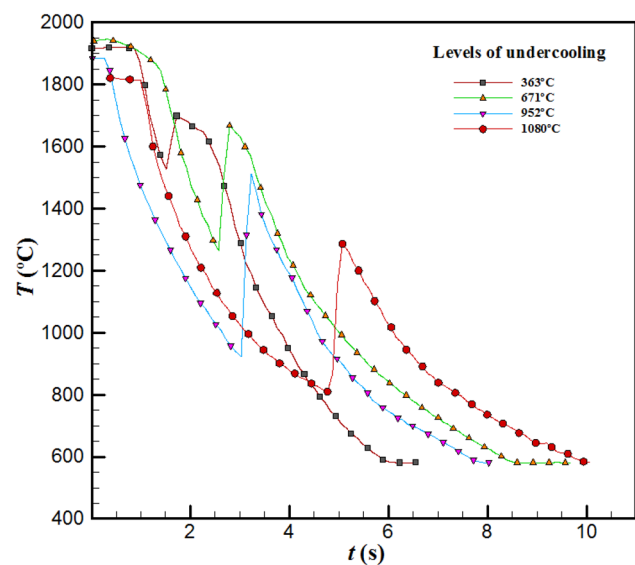
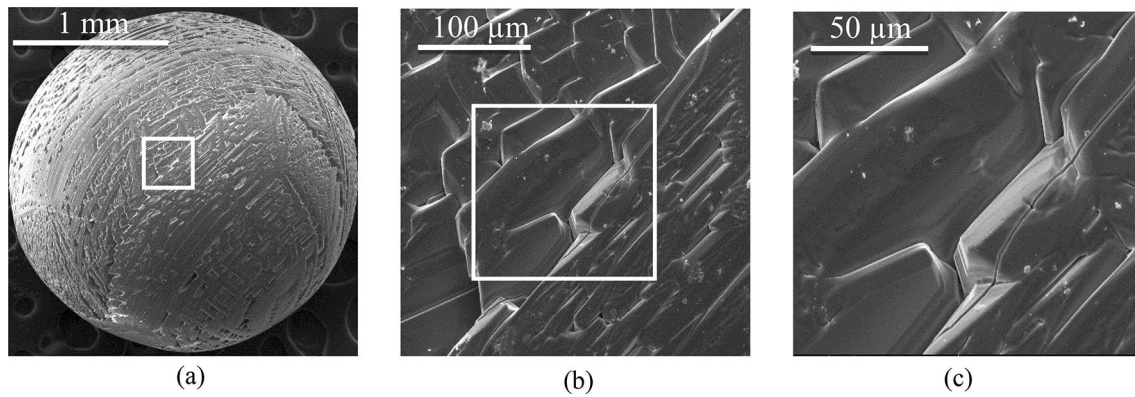


Fig. 3 Cooling curves for different levels of undercooling

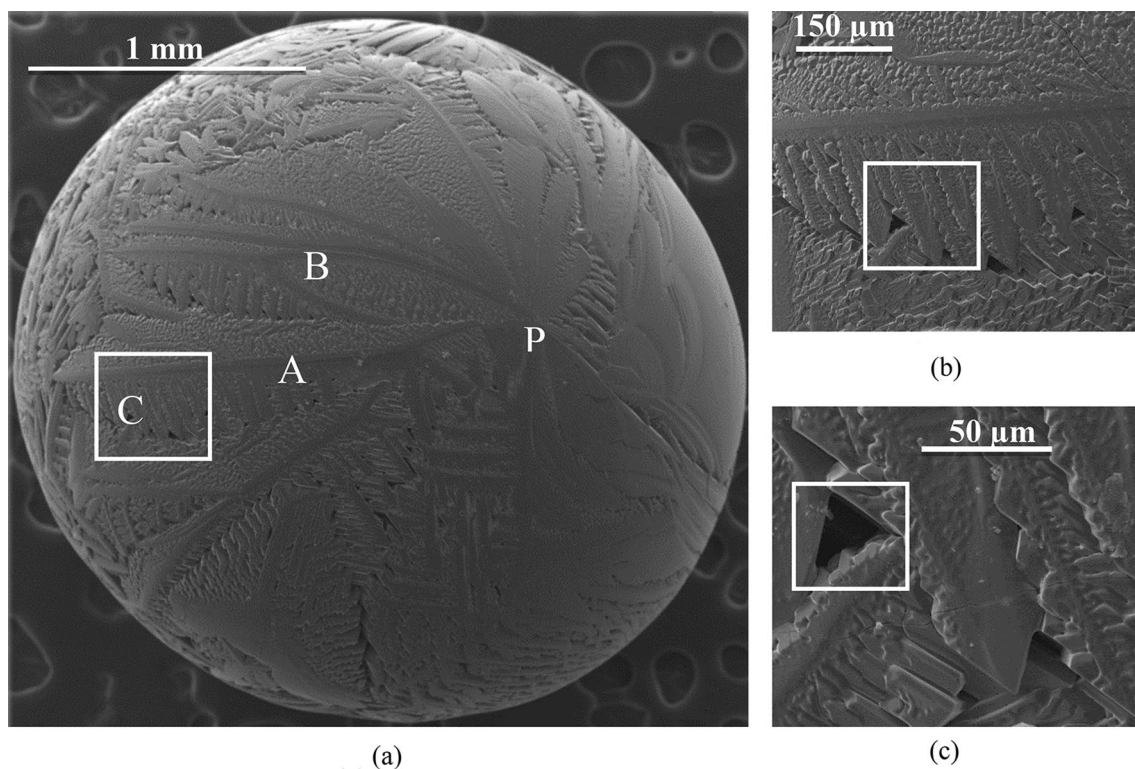
up to  $1100^\circ\text{C}$  (Fig. 2). Figure 3 shows clear demarcations between different cooling curves in which the onset of nucleation occurs at different temperatures. Hence, each of these cooling curves marks a different undercooling value, thus allowing an investigation of a range of surface features. It is to be noted from the figure that the recalescence temperature peak varies as the level of undercooling is varied in the experiments. These observations find support in the works of Xu et al. [24] and Shukla et al. [25] wherein the authors reported that the recalescence is altered when the levels of undercooling are changed. The concerned literature suggests that the recalescence does vary (including significant changes in the thermo-physical properties of the sample<sup>2</sup>), and this appears to be quite amplified in the present study due to the nature of extreme undercooling levels.

Figure 4 shows the details of the surface features of the forsterite spherule after the completion of the crystallization process. The undercooling achieved in this case is  $626^\circ\text{C}$ . The surface shows presence of faceted branching of the solidification morphology (Fig. 4a). This is further

<sup>2</sup> Literature suggests that when the level of undercooling approaches or exceeds the hypercooling limit, the change in the enthalpy of fusion is modified as  $\Delta H_f = C_p^L (T_m - T_{hyp})$  where  $C_p^L$  is the temperature dependent specific heat,  $\Delta H_f$  is the latent heat of fusion,  $T_m$  is the melting temperature and  $T_{hyp}$  is the hypercooling temperature [26]. The specific heat is also expected to increase (almost double) as the undercooled levels rise [27]. Thus, as has also been discussed by Perepezko [28], the analysis of crystallization of highly undercooled melts is highly challenging owing to the difficulties in obtaining the experimental kinetic and thermodynamic data.



**Fig. 4** SEM images of **a** solidified spherule for undercooling  $\Delta T=626\text{ }^{\circ}\text{C}$  showing faceted features, **b** Enlarged view of square box in Fig. 4a, **c** Enlarged view of square box in Fig. 4b showing faceted features



**Fig. 5** SEM images showing **a** dendritic morphology at undercooling of  $770\text{ }^{\circ}\text{C}$ . **b** Enlarged view of square box in Fig. 5a. **c** Enlarged view of square box in Fig. 5b where at first glance square in the Fig. c shows shrinkage void

confirmed by examining at a much higher magnification (Fig. 4b, c). It is to be mentioned here that, in addition to surface features, SEM analyses of thin section of the solidified samples were also carried out. These observations were found to be in good agreement with surface morphologies of the solidified samples.

In Fig. 5a, the solidified spherules at undercooling of  $770\text{ }^{\circ}\text{C}$  are shown, in which one can distinctly observe

some major dendrite trunks (A and B) with overgrowth of secondary dendrite arms (region 'C' in Fig. 5a). All these major primary arms emanate from a point P and propagate randomly in various directions. Expanded view of this C region (Fig. 5b) also shows how crystals of thickness

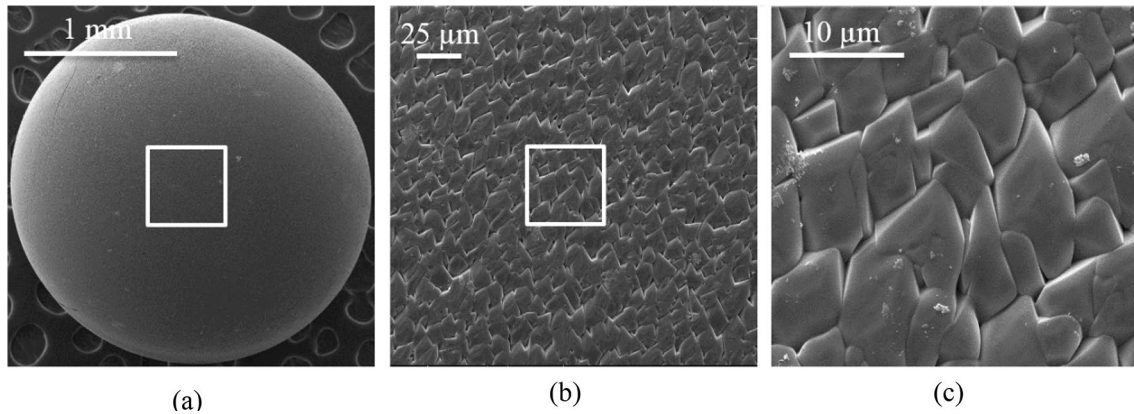


**Fig. 6** SEM image of **a** solidified spherule for undercooling  $\Delta T = 970$  °C. **b** Enlarged view of square box in Fig. 6a. **c** Enlarged view of square box in Fig. 6c showing faceted features

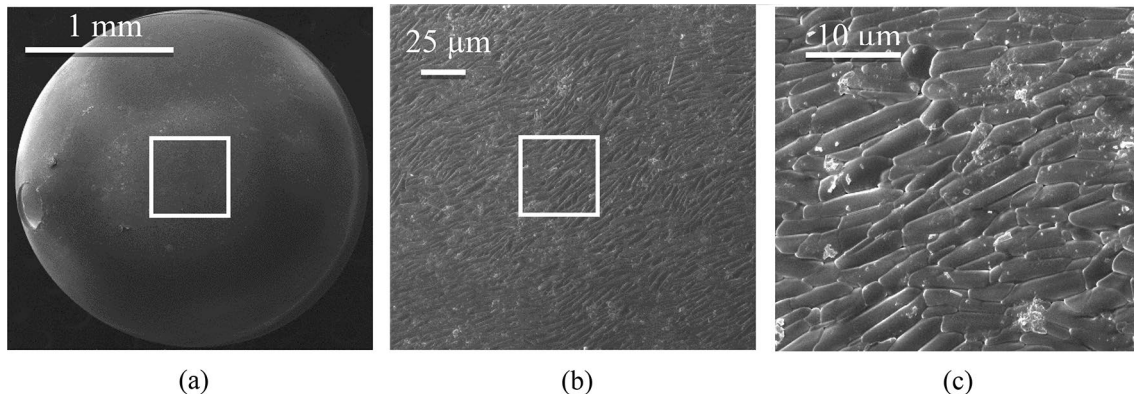


**Fig. 7** SEM images of **a** solidified spherule for undercooling  $\Delta T = 1080$  °C **b** Enlarged view of square box in Fig. 7a, **c** Enlarged view of square box in Fig. 7b

restricted to a few microns, act as the secondary arm of dendrite. When the same is zoomed, voids due to the shrinkage of the material can be clearly seen from Fig. 5c. The SEM observations performed on the external surface of the solidified samples provide possible signatures of the highly branched dendritic microstructure that are in good agreement with those reported in the literature, wherein similar experiments performed with samples supported through contact<sup>3</sup> by Faure et al. [19].

When even higher levels of undercooling were achieved, a morphological difference became evident. The solidified spherule in Fig. 6a, which corresponds to

an undercooling level of  $\Delta T \approx 970$  °C, does not show any clear indication of branched morphology as that of Fig. 4a or Fig. 5a. The physical mechanism which leads to the morphological transition from faceted dendrites at lower undercooling to non-dendritic features at high undercooling has not been fully understood. Yet, the mechanism of formation of such unbranched features for significantly higher undercooling can be understood from nucleation and growth processes. For higher undercooling, large number of nuclei are formed. Therefore, these large undercooling values also results in higher nucleation rates. Hence after sufficient enlargement, large number of faceted features can be partially seen from Fig. 6b and upon further enlarging, faceted features can be completely recognized from Fig. 6c.

The morphological features seen in Fig. 7 are completely different from those obtained in Fig. 4a or Fig. 5a (in which faceted dendrites were to be seen) suggesting the possibility of homogeneous nucleation. Here

<sup>3</sup> As per the available literature, such techniques make use of an external solid substrate, or a wire loop (made of platinum/iridium), on which the sample is placed, hence is in contact with the sample holder [6].

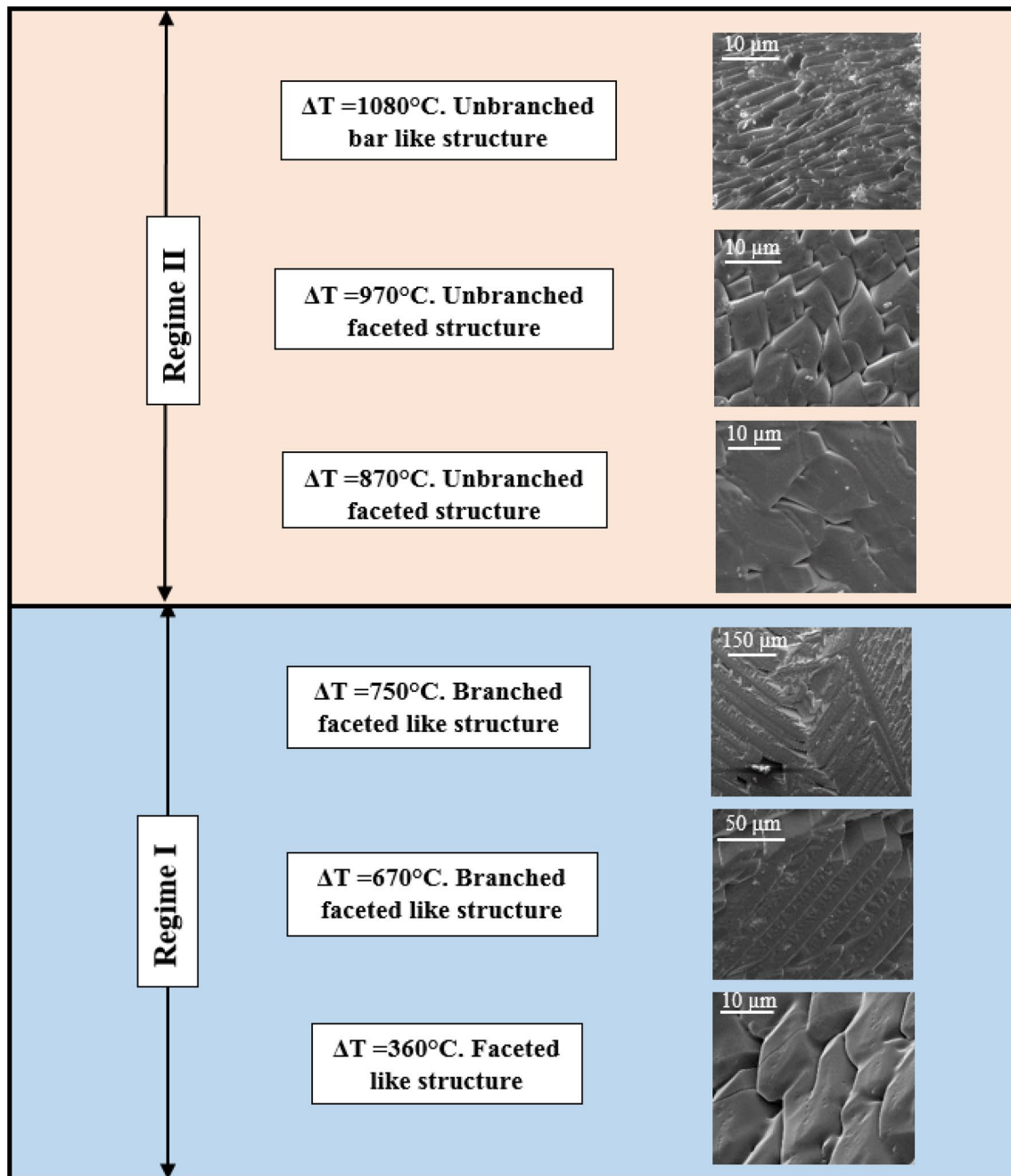


**Fig. 8** Morphological transition of magnesium silicate for various levels of undercooling

nucleation appears to have been taken place at a large number of sites, which eventually resulted in a strikingly even distribution of fine features, which are consistently about  $10\ \mu\text{m}$  in size, subjected to the maximum levels of undercooling that could be achieved in the experiments reported (shown in the Fig. 7). This maximum level of undercooling corresponds to  $\Delta T \approx 1080^\circ\text{C}$ . It is to be mentioned that slight variations in heating and cooling

rates, the flow rate of the levitation gas, could have also resulted in slight variation in the values of undercooling. More importantly, in comparison to the above, the vast difference in the nature of features observed for the relatively lower undercooling values indicate that the nucleation rate drastically changes when a threshold undercooling limit is exceeded.

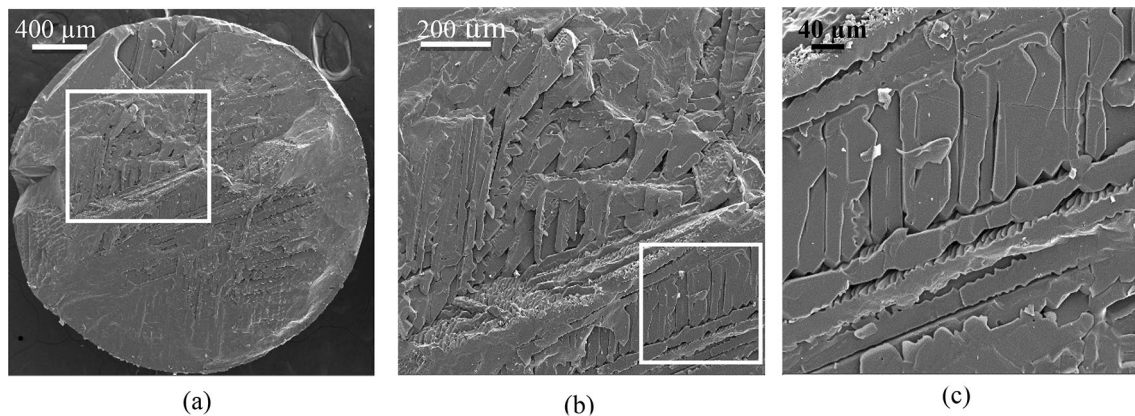


**Fig. 9** SEM images of **a** sample frozen in the low undercooling regime **b** Enlarged view of square box in Fig. 9a, **c** Enlarged view of square box in Fig. 9b showing faceted features for low undercooling regime

### 3.2 Regime map

Figure 8 depicts the morphological transition of magnesium silicate with varying levels of undercooling employed for solidifying the molten droplets. The range of undercooling ( $\Delta T$ ) obtained in the experiments is between 360 to 1100 °C. Based on the SEM observations of these solidified samples as presented above, the morphological transition can be broadly classified into two major regimes on the basis of the level of undercooling:

1. Branched faceted regime between undercooling ( $\Delta T$ ) of 360 and 800 °C
2. Unbranched faceted regime above the undercooling ( $\Delta T$ ) of 800 °C.

These distinct regimes have been presented in Fig. 8. The change in undercooling levels indicates that there is a significant morphological transition. With reference to Fig. 8, Regime I shows branched faceted features, which lies between undercooling ( $\Delta T$ ) level of 360 and 800 °C. It should be noted here that, within the experimental uncertainties associated with the measurement of the instantaneous temperature of the solidifying sample, the lowest level of undercooling that could be achieved in the present set of experiments is somewhat closer to the theoretical value of hypercooling limit of pure forsterite sample ( $\Delta T = 425$  °C). The regimes (1 and 2 as listed above) also suggest the existence of an abrupt change in the crystallization kinetics, when large levels of undercooling ( $> \sim 800$  °C) are achieved i.e. when the crystallization takes place at absolute temperatures that are lesser than  $\sim 1100$  °C. The realization of branched faceted features in this regime also suggests the possibility of heterogeneous nucleation even after the fact that the solidifying sample is maintained under levitated condition.

The possible sources of heterogeneous nucleation may be the presence of impurities and/or the left-over partially melted micron-sized silicate particles in the otherwise molten droplet of the sample volume. Possibility of such factors that lead to the onset of heterogeneous nucleation in experiments conducted under non-contact conditions has also been discussed in the works reported by Nagashima et al. [6] in the context of chondrule crystallization and forsterite ( $Mg_2SiO_4$ )-based crystallization experiments. However, further investigation of the presence of any small nucleating site is needed, as the heterogeneous nucleation is generally very unlikely to occur at such undercooling values, particularly beyond the hypercooling limit.

Regime II corresponds to the realization of non-dendritic features obtained as a result of solidification phenomenon above an undercooling ( $\Delta T$ ) level of 800 °C. The morphological features seen in Regime II are completely different from those obtained in Regime I (in which faceted dendrites were to be seen) suggesting the possibility of homogeneous nucleation.

Further investigations have been performed to confirm the inner features of the solidified spherules. The spherules have been cut approximately at its mid-plane, and the SEM image of the same (sectioned samples) is shown in Fig. 9a for regime-I. Sufficient magnification clearly shows the branching of the features in Fig. 9b, c. A difference in the extent of branching is likely to exist as the cooling rates would vary from the surface to internal locations.

When the samples from regime-II were examined for internal features, no branched structures were observed (see Fig. 10a). The marked square in Fig. 10a is enlarged in Fig. 10b which showed a cluster of facets. With further enhancement in magnification of the square box in Fig. 10b, edges of a facet can be noticed (see Fig. 10c). It

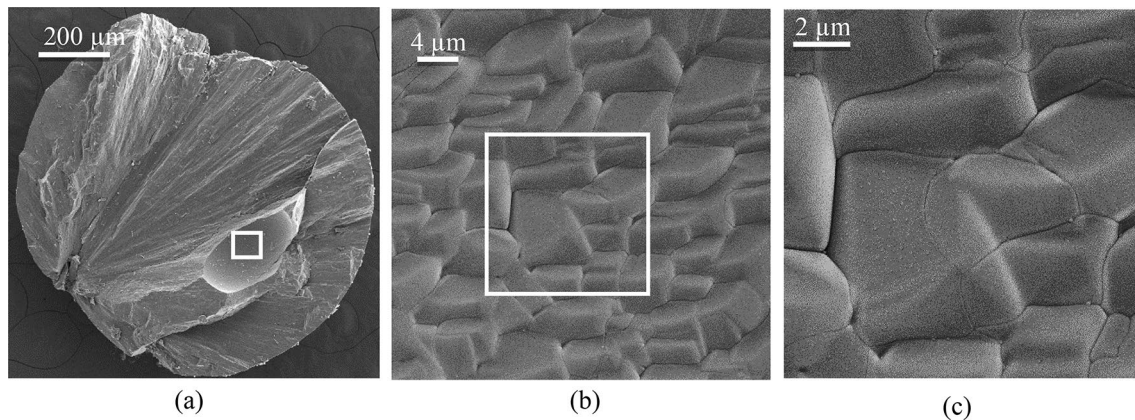
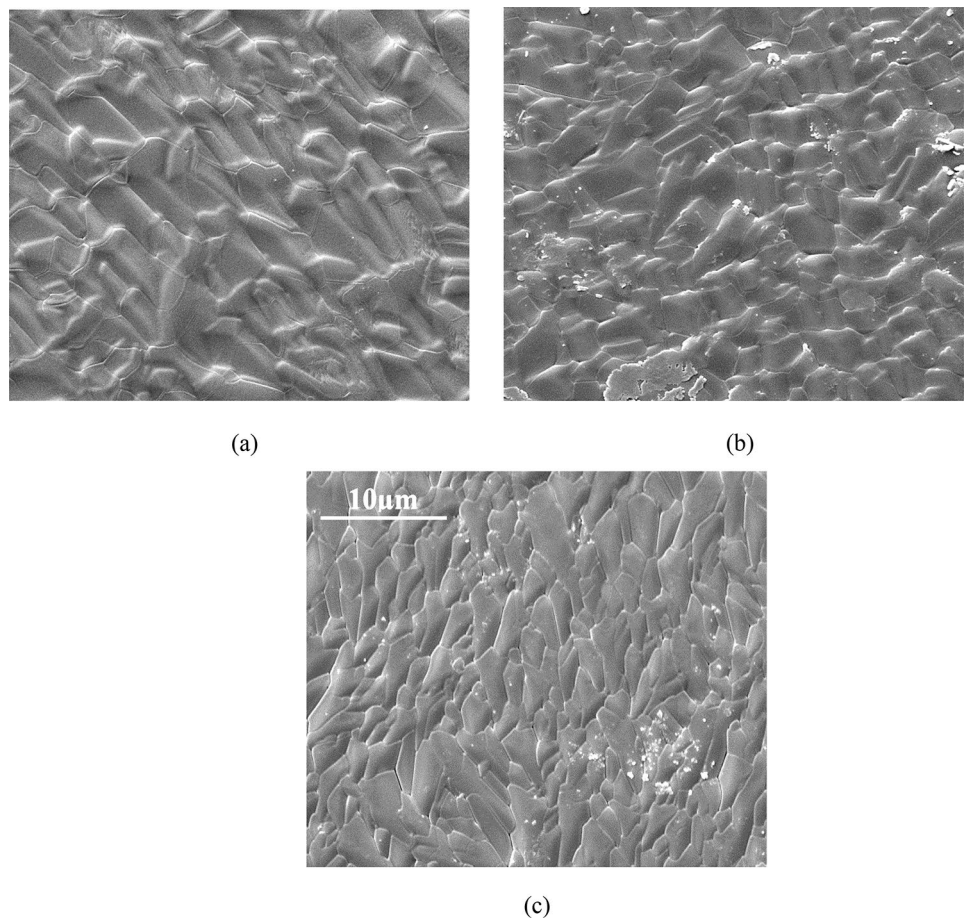


**Fig. 10** SEM images of **a** sample frozen in the high undercooling regime **b** Enlarged view of square box in Fig. 10a, **c** Enlarged view of square box in Fig. 10b showing faceted features for high undercooling regime

**Fig. 11** SEM images for cooling rates of 30, 100 and 180 °C/s and its undercooling 1012, 1028 and 1133 °C respectively for figures starting from **a–c**. For the level maximum undercooling achieved, (1133 °C), the sample displays extremely fine microstructures **c** as compared to other two microstructures shown in **(a)** and **(b)**



is evident from this figure that only faceted features have been found in this regime as compared to the branched features of the low undercooling regime. It has been found that features which are observed inside the solidified spherules for both low undercooling as well as the high undercooling regimes are in good agreement with outside surface features.

### 3.3 Observations of surface features at various levels of cooling rate

Cooling rate is one of the important parameters affecting the morphological (as well as compositional) features of the solidified samples. For instance, in the context of planetary science, one of the theories widely floated in

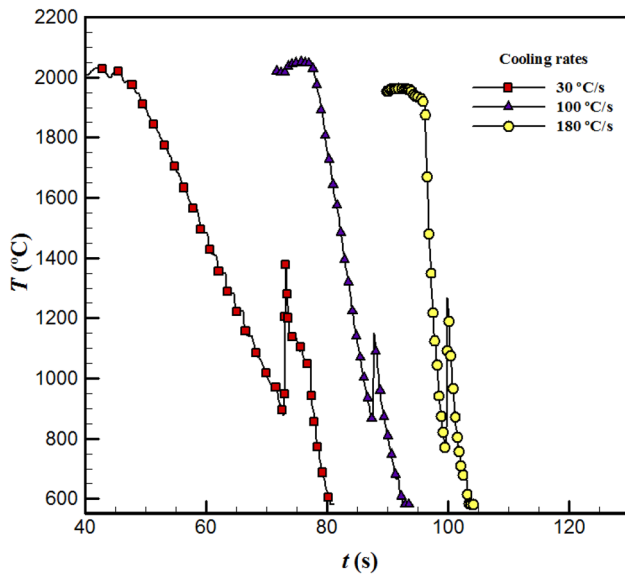


**Fig. 12** Cooling curves for experiments conducted at different cooling rates

the literature indicates towards the possibility of chondrule crystallization as a result of slow cooling rates that vary between  $\sim 10$ – $1000$   $^{\circ}\text{C}/\text{h}$  [20, 21]. However, in these reported studies, the chondrule crystallization experiments were carried out using electric furnaces, which limit the realization of extremely high cooling rates in the order of ( $\sim 100$   $^{\circ}\text{C}/\text{s}$ ), as recommended by astrophysical models [22] in the context of chondrule crystallization phenomenon. In this context, the present experimental methodology becomes important as varying levels of cooling rates can be achieved by controlling the output power of the  $\text{CO}_2$  laser. This section discusses the morphological transition of forsterite samples ( $\text{Mg}_2\text{SiO}_4$ ) as a function of the cooling rates (30, 100 and 180  $^{\circ}\text{C}/\text{s}$ ).

From the SEM images shown in Fig. 11a, b, c, one can observe that the microstructures tend to become finer with increasing cooling rates, irrespective of the level of undercooling employed in the experiments. It can also be seen from Fig. 12, that there is no significant effect on the undercooling even though the cooling rate employed to the solidified sample is increased. On the other hand, the maximum undercooling (1133  $^{\circ}\text{C}$ ) achieved at the highest level of cooling rate employed (180  $^{\circ}\text{C}/\text{s}$ ) in the experiments leads to the realization of extremely fine microstructures compared to the other two microstructures shown in Fig. 11a, b. The realization

of very fine microstructures at higher levels of cooling rates is attributed to the rapid advancement (movement) of the solid–liquid interface as the cooling rate is increased, which has been well documented in the literature. These observations also imply that both undercooling, as well as cooling rates, have affected the microstructures significantly, while Tsuchiyama et al. [23] suggested that the cooling rate may affect the transition in microstructure but is subordinate to compositional effect (It is to be noted here that experiments reported by Tsuchiyama et al. [23] were performed for relatively lower cooling rates).

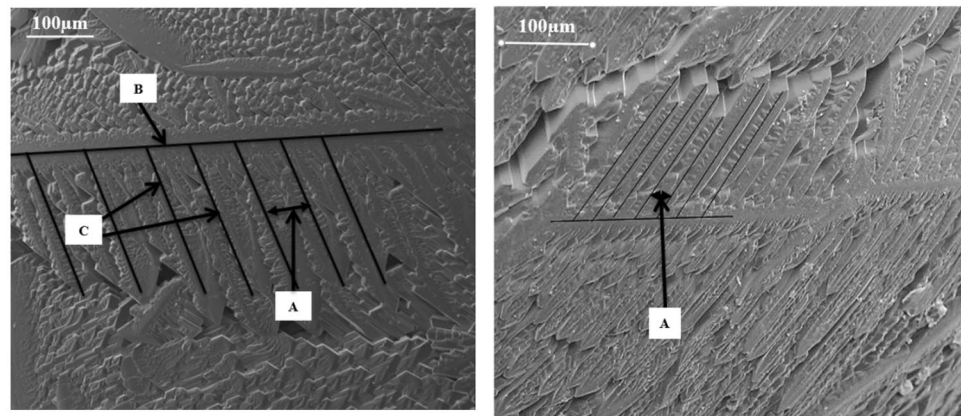
### 3.3.1 Discussion on SDAS (secondary dendrite arm spacing)

Study of surface features obtained in Regime I can be further extended to determine the secondary dendrite arm spacing. In Fig. 13a, b, representative images of dendrite structure containing primary and secondary arms have been shown. These representative images reflect slightly uneven spacing between secondary dendrite arms. For this reason, as a first-hand approximation, average value of these different values of SDAS (secondary dendrite arm spacing) has been considered. The structural results presented in Fig. 13c show that the secondary dendrite arm spacing (SDAS) decreases almost in a linear manner with increasing cooling rate. The observed trend may be attributed to the ease with which the heat from the surface of the solidifying sample gets dissipated at higher levels of cooling rate.

## 4 Conclusions

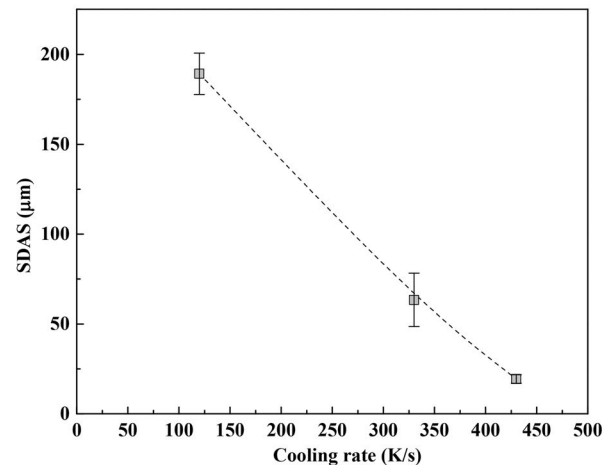
Solidification experiments under non-contact conditions were performed for investigating the morphological transition of non-metallic systems (forsterite spherules as the model material) at various undercooling levels and cooling rates. The solidified spherules were examined for observing surface feature morphology and quantification using SEM technique. Depending on the level of undercooling employed, the experimental findings revealed the existence of two broad regimes of microstructure formation and the resulting feature morphologies. For relatively lower undercooling regime (between 360–800  $^{\circ}\text{C}$ ), highly branched faceted features were observed, whereas for

**Fig. 13** SEM images for **a** cooling rate of 330 °C/s where SDAS is 65  $\mu\text{m}$ . Also point A refers to secondary dendrite arm spacing, B is primary arm of dendrite and C is secondary arm of dendrite. **b** SEM image for cooling rate of 420 °C/s where SDAS is 23  $\mu\text{m}$ . Also point A refers to secondary dendrite arm spacing **c** Variation of SDAS versus cooling rate



(a)

(b)



(c)

much higher undercooling values i.e. above 800° C, ultra-fine unbranched faceted structures were to be seen. The nature of consistent unbranched morphological features for the regime-II strongly suggests the existence of a large nucleation rate. The experiments revealed, a new observation of morphological transition at extremely high undercooling limits which have never been explored before. Further, the feature sizes showed dependence on the cooling rate, but interestingly, the observed regimes were largely unaffected by the changes in the cooling rates. More detailed studies are required to carefully explore the mechanisms of nucleation beyond the hypercooling limit.

**Acknowledgements** This project was supported by Department of Science and Technology (DST), India under the Swarnajayanti Fellowship scheme (Grant ID: RD/0115-DSTFL80-005). The authors acknowledge the support received from DST, India. Assistance received from SAIF, IIT Bombay in performing SEM analysis of the solidified samples is also gratefully acknowledged. GS is grateful to Dr. Kaushik Choudhury for imparting initial training on handling the aerodynamic levitation system and the associated instrumentation.

## Compliance with ethical standards

**Conflict of interest** On behalf of all authors, the corresponding author states that there is no conflict of interest.

**Open Access** This article is licensed under a Creative Commons Attribution 4.0 International License, which permits use, sharing, adaptation, distribution and reproduction in any medium or format, as long as you give appropriate credit to the original author(s) and the source, provide a link to the Creative Commons licence, and indicate if changes were made. The images or other third party material in this article are included in the article's Creative Commons licence, unless indicated otherwise in a credit line to the material. If material is not included in the article's Creative Commons licence and your intended use is not permitted by statutory regulation or exceeds the permitted use, you will need to obtain permission directly from the copyright holder. To view a copy of this licence, visit <http://creativecommons.org/licenses/by/4.0/>.

## References

1. Lü P, Zhou K, Wang HP (2016) Evidence for the transition from primary to peritectic phase growth during solidification of

- undercooled Ni-Zr alloy levitated by electromagnetic field. *Sci Rep* 6:39042. <https://doi.org/10.1038/srep39042>
- Binder S, Galenko PK, Herlach DM (2013) Faceting of a rough solid-liquid interface of a metal induced by forced convection. *Philos Mag Lett* 93:608–617. <https://doi.org/10.1080/09500839.2013.830201>
  - Watanabe K, Nagayama K, Kuribayashi K (2011) Morphological transition in crystallization of Si from undercooled melt. *J Phys.* <https://doi.org/10.1088/1742-6596/327/1/012018>
  - Aoyama T, Kuribayashi K (2000) Influence of undercooling on solid/liquid interface morphology in semiconductors. *Acta Mater* 48:3739–3744. [https://doi.org/10.1016/S1359-6454\(00\)00164-6](https://doi.org/10.1016/S1359-6454(00)00164-6)
  - Jones RH, Grossman JN, Rubin AE (2005) Chemical Mineralogical and isotopic properties of chondrules : clues to their origin. *Chondrite Protoplanetary Disk* 341:251–285
  - Nagashima K, Tsukamoto K, Satoh H, Kobatake H, Dold P (2006) Reproduction of chondrules from levitated, hypercooled melts. *J Cryst Growth* 293:193. <https://doi.org/10.1016/j.jcrysgro.2006.01.064>
  - Zanda B (2004) Chondrules, earth planet. *Sci Lett* 224:1–17. <https://doi.org/10.1016/j.epsl.2004.05.005>
  - Libourel G, Portail M (2018) Chondrules as direct thermochemical sensors of solar protoplanetary disk gas. *Sci Adv.* <https://doi.org/10.1126/sciadv.aar3321>
  - Srivastava A, Inatomi Y, Tsukamoto K, Maki T, Miura H (2010) In situ visualization of crystallization inside high temperature silicate melts. *J Appl Phys* 107:1–7. <https://doi.org/10.1063/1.3406149>
  - Pack A, Kremer K, Albrecht N, Simon K, Kronz A (2010) Description of an aerodynamic levitation apparatus with applications in earth sciences. *Geochem Trans* 11:1–16. <https://doi.org/10.1186/1467-4866-11-4>
  - Beitz E, Blum J, Mathieu R, Pack A, Hezel DC (2013) Experimental investigation of the nebular formation of chondrule rims and the formation of chondrite parent bodies. *Geochim Cosmochim Acta* 116:41–51. <https://doi.org/10.1016/j.gca.2012.04.059>
  - Cervantes-de la Cruz KE, Gutiérrez FO, Viñas JS, Peralta AS, Reyes Salas MA, B.S. ángeles García, M. del C. Macías Romo, C. Linares-López, (2015) Experimental chondrules by melting samples of olivine, clays and carbon with a CO<sub>2</sub> laser. *Bol La Soc Geol Mex* 67:401–412
  - Faure F, Trolliard G, Nicollet C, Montel JM (2003) A developmental model of olivine morphology as a function of the cooling rate and the degree of undercooling. *Contrib Miner Petrol* 145:251–263. <https://doi.org/10.1007/s00410-003-0449-y>
  - Miura H, Ninagawa K, Tsukamoto K, Nishido H, Kimura Y, Kayama M, Gucsik A (2011) Cathodoluminescence microcharacterization of forsterite in the chondrule experimentally grown under super cooling. *J Lumin* 132:1041–1047. <https://doi.org/10.1016/j.jlumin.2011.12.011>
  - Nicollet C, Faure F, Schiano P, Soulestin B, Trolliard G (2006) Textural evolution of polyhedral olivine experiencing rapid cooling rates. *Contrib Miner Petrol* 153:405–416. <https://doi.org/10.1007/s00410-006-0154-8>
  - Faure F, Trolliard G, Soulestin B (2003) TEM investigation of forsterite dendrites. *Am Mineral* 88:1241–1450
  - Miura H, Yokoyama E, Nagashima K, Tsukamoto K, Srivastava A (2010) Phase-field simulation for crystallization of a highly supercooled forsterite-chondrule melt droplet. *J Appl Phys.* <https://doi.org/10.1063/1.3504655>
  - Yokoyama E, Tsukamoto K, Miura H, Srivastava A, Nagashima K (2012) A new constraint for chondrule formation: condition for the rim formation of barred-olivine textures. *Earth, Planet Sp* 63:1087–1096. <https://doi.org/10.5047/eps.2011.06.004>
  - Faure F, Schiano P (2005) Experimental investigation of equilibration conditions during forsterite growth and melt inclusion formation, earth planet. *Sci Lett* 236:882–898. <https://doi.org/10.1016/j.epsl.2005.04.050>
  - Tsuchiyama A, Nagahara H (1981) Effect of precooling thermal history and cooling rate on the texture of chondrules: a preliminary report. *Mem Nat Inst Polar Res* 20:175
  - Lofgren GE (1996) A dynamic crystallization model for chondrule melts chondrules protoplanetary disk. Cambridge Univ Press, Cambridge, p 187
  - Iida A, Nakamoto T, Susa H, Nakagawa Y (2001) A shock heating model for chondrule formation in a protoplanetary disk. *Icarus* 153:430–450. <https://doi.org/10.1006/icar.2001.6682>
  - Tsuchiyama A, Nagahara H, Kushiro I (1980) Experimental reproduction of textures of chondrules, earth Planet. *Sci Lett* 48:155–165. [https://doi.org/10.1016/0012-821X\(80\)90178-8](https://doi.org/10.1016/0012-821X(80)90178-8)
  - Xu J, Yang T, Li Z, Wang X, Xiao Y, Jian Z (2020) The recalescence rate of cooling curve for undercooled solidification. *Sci Rep* 10:1–5. <https://doi.org/10.1038/s41598-019-56079-6>
  - Shukla P, Mandal RK, Ojha SN (2001) Non-equilibrium solidification of undercooled droplets during atomization process. *Bull Mater Sci* 24:547–554. <https://doi.org/10.1007/BF02706729>
  - Volkman T, Wilde G, Willnecker R, Herlach DM (1998) Nonequilibrium solidification of hypercooled Co-Pd melts. *J Appl Phys* 83:3028–3034. <https://doi.org/10.1063/1.367057>
  - Gillet P, Richet P, Guyot F, Fiquet G (1991) High-temperature thermodynamic properties of forsterite. *J Geophys Res* 96(B7):11805–11816
  - Perepezko JH (1993) Solidification of highly supercooled liquid metals and alloys. *J Non-Cryst Solids* 156–158:463–472

**Publisher's Note** Springer Nature remains neutral with regard to jurisdictional claims in published maps and institutional affiliations.